REPORT DOCUMENTATION PAGE

Form Approved OMB NO. 0704-0188

1. REPORT DATE (DD-MM-YYYY)	2. REPORT TYPE	3. DATES COVERED (From - To)
20-07-2015	Final Report	1-Feb-2014 - 30-Apr-2015

4. TITLE AND SUBTITLE
Final Report: Acquisition of a High-Resolution High-Intensity X-ray Diffractometer for Research and Education

5a. CONTRACT NUMBER
W911NF-14-1-0072

5b. GRANT NUMBER

5c. PROGRAM ELEMENT NUMBER
206022

6. AUTHORS
Stefan Zollner

5d. PROJECT NUMBER

5e. TASK NUMBER

5f. WORK UNIT NUMBER

7. PERFORMING ORGANIZATION NAMES AND ADDRESSES
New Mexico State University
PO Box 30002, MSC OGC
Anderson Hall E1200, Espina and Stewart Streets
Las Cruces, NM 88003 -8002

8. PERFORMING ORGANIZATION REPORT NUMBER

9. SPONSORING/MONITORING AGENCY NAME(S) AND ADDRESS (ES)
U.S. Army Research Office
P.O. Box 12211
Research Triangle Park, NC 27709-2211

10. SPONSOR/MONITOR'S ACRONYM(S)
ARO

11. SPONSOR/MONITOR'S REPORT NUMBER(S)
64744-EL-REP.1

12. DISTRIBUTION AVAILIBILITY STATEMENT
Approved for Public Release; Distribution Unlimited

13. SUPPLEMENTARY NOTES
The views, opinions and/or findings contained in this report are those of the author(s) and should not contrued as an official Department of the Army position, policy or decision, unless so designated by other documentation.

14. ABSTRACT
NMSU acquired a high-resolution high-intensity x-ray diffractometer for research and education. A PANalytical Empyrean system was acquired and installed, with three types of incident beam optics, two sample cradles, and two detectors. This instrument allows powder diffraction, x-ray reflectivity, texture and pole figure, and small-angle x-ray scattering measurements. It is also suitable for high-resolution diffraction, including triple-axis reciprocal space maps for symmetric and asymmetric Bragg reflections. A one-dimensional line detector significantly decreases data acquisition time for certain measurements. Commercial software allows data analysis, modeling, and fitting of

15. SUBJECT TERMS
X-ray diffraction; germanium-tin alloys;

16. SECURITY CLASSIFICATION OF:			17. LIMITATION OF ABSTRACT	15. NUMBER OF PAGES	19a. NAME OF RESPONSIBLE PERSON
a. REPORT	b. ABSTRACT	c. THIS PAGE			Stefan Zollner
UU	UU	UU	UU		19b. TELEPHONE NUMBER 575-646-7627

Report Title

Final Report: Acquisition of a High-Resolution High-Intensity X-ray Diffractometer for Research and Education

ABSTRACT

NMSU acquired a high-resolution high-intensity x-ray diffractometer for research and education. A PANalytical Empyrean system was acquired and installed, with three types of incident beam optics, two sample cradles, and two detectors. This instrument allows powder diffraction, x-ray reflectivity, texture and pole figure, and small-angle x-ray scattering measurements. It is also suitable for high-resolution diffraction, including triple-axis reciprocal space maps for symmetric and asymmetric Bragg reflections. A one-dimensional line detector significantly decreases data acquisition time for certain measurements. Commercial software allows data analysis, modeling, and fitting of lattice parameters. The instrument currently has 23 authorized users from the departments of Physics, Chemistry and Biochemistry, Chemical and Materials Engineering (5 faculty, 15 graduate students, 3 undergraduate students). In the spring of 2015, the instrument was used for an instructional laboratory course in modern physics. The PI will teach a course on x-ray diffraction in the fall of 2015. The instrument has been fully tested for some of its capabilities and testing is in progress for others. Comprehensive data were acquired for pseudomorphic germanium-tin alloys grown on germanium by molecular beam epitaxy. Other projects involve nickel alloy thin films and related silicides, complex metal oxides, ferroelectrics, and powders of nanoparticles.

Enter List of papers submitted or published that acknowledge ARO support from the start of the project to the date of this printing. List the papers, including journal references, in the following categories:

(a) Papers published in peer-reviewed journals (N/A for none)

Received	Paper

TOTAL:

Number of Papers published in peer-reviewed journals:

(b) Papers published in non-peer-reviewed journals (N/A for none)

Received	Paper

TOTAL:

Number of Papers published in non peer-reviewed journals:

(c) Presentations

Number of Presentations: 0.00

Non Peer-Reviewed Conference Proceeding publications (other than abstracts):

Received Paper

TOTAL:

Number of Non Peer-Reviewed Conference Proceeding publications (other than abstracts):

Peer-Reviewed Conference Proceeding publications (other than abstracts):

Received Paper

TOTAL:

Number of Peer-Reviewed Conference Proceeding publications (other than abstracts):

(d) Manuscripts

Received Paper

TOTAL:

Number of Manuscripts:

Books

Received Book

TOTAL:

Received Book Chapter

TOTAL:

Patents Submitted

Patents Awarded

Awards

Graduate Students

NAME	PERCENT_SUPPORTED	Discipline
Dennis P. Trujillo	0.00	
Nalin Fernando	0.00	
Nuwanjula Samarasingha	0.00	
FTE Equivalent:	**0.00**	
Total Number:	**3**	

Names of Post Doctorates

NAME	PERCENT_SUPPORTED
FTE Equivalent:	
Total Number:	

Names of Faculty Supported

NAME	PERCENT_SUPPORTED	National Academy Member
Stefan Zollner	0.00	
FTE Equivalent:	**0.00**	
Total Number:	**1**	

Names of Under Graduate students supported

NAME	PERCENT_SUPPORTED	Discipline
Jaime Moya	0.00	Physics
Luis Barrera	0.00	Physics
Khadijih N. Mitchell	0.00	Physics
FTE Equivalent:	**0.00**	
Total Number:	**3**	

Student Metrics

This section only applies to graduating undergraduates supported by this agreement in this reporting period

The number of undergraduates funded by this agreement who graduated during this period: 0.00

The number of undergraduates funded by this agreement who graduated during this period with a degree in science, mathematics, engineering, or technology fields:..... 0.00

The number of undergraduates funded by your agreement who graduated during this period and will continue to pursue a graduate or Ph.D. degree in science, mathematics, engineering, or technology fields:..... 0.00

Number of graduating undergraduates who achieved a 3.5 GPA to 4.0 (4.0 max scale):..... 0.00

Number of graduating undergraduates funded by a DoD funded Center of Excellence grant for Education, Research and Engineering:..... 0.00

The number of undergraduates funded by your agreement who graduated during this period and intend to work for the Department of Defense 0.00

The number of undergraduates funded by your agreement who graduated during this period and will receive scholarships or fellowships for further studies in science, mathematics, engineering or technology fields: 0.00

Names of Personnel receiving masters degrees

NAME
Total Number:

Names of personnel receiving PHDs

NAME
Total Number:

Names of other research staff

NAME	PERCENT_SUPPORTED

FTE Equivalent:
Total Number:

Sub Contractors (DD882)

Inventions (DD882)

Scientific Progress

See attachment.

Technology Transfer

Final Report: Acquisition of a High-Resolution High-Intensity X-ray Diffractometer for Research and Education

Stefan Zollner, Department of Physics, New Mexico State University, Las Cruces, NM

Summary of Acquisition and Installation:

New Mexico State University acquired a PANalytical Empyrean x-ray diffractometer with details of the configuration as shown in Table I. Figures 1 and 2 show the overall instrument and a magnified image of the incident beam optic, sample stage, and diffracted beam optic, respectively. The instrument has a full one-year warranty ending on December 31st, 2015. The x-ray tube, goniometer, and mirrors are covered with an extended academic 78 month warranty. Table II shows an overview of our progress towards mastery of the instrument and its capabilities.

To install the instrument, NMSU Facilities & Services added a high-power 208 V switch to the laboratory. Cooling of the x-ray tube is achieved with a Haskris air chiller. Therefore, no water is consumed for cooling. The exhaust air from the chiller is routed directly into the plenum above the ceiling tiles, where it is accepted by the air handlers. A floor sink was deemed necessary in case of water spills. A key card reader was installed to allow access to authorized users. A web site http://xrd.research.nmsu.edu was built to advertise the instrument to the NMSU community and to allow users to book time on the instrument.

The x-ray source is a 2.2 kW Cu anode long fine focus ceramic tube, typically operated at 45 kV and 40 mA. A Ni filter (for reducing Cu K_β radiation) and Cu attenuation filters are provided. Beam masks with 2 mm, 4 mm, 10 mm, and 20 mm are used dependent on sample size. Soller slits of 0.04 radians can be used in the incident or diffracted beam path. In addition to various divergence and anti-scatter slits, special slits are provided for x-ray reflectance, microbeam point-optic, and small angle x-ray scattering (SAXS) measurements. The instrument has two separate diffracted beam paths, allowing two detectors to be mounted simultaneously. This allows fast low- or medium resolution measurements (with the 1-D detector) and high-resolution triple-axis measurements (with the Xe proportional detector) to be performed without any hardware changes. All components are prealigned and easy to switch with the need for realignment. Powders can be mounted for transmission or reflection measurements on a Si zero-background substrate, using Kapton foils, or metal sample holders with a recess holding the powder. A dial gauge helps to find the right sample height. Reference samples were provided for powder diffraction (sintered poly-Si disk), high-resolution diffraction (Si 111), texture (Cu), reflectivity (Cr), and SAXS (nanoparticles with ZnO and TiO_2).

A computer and printer shipped with the instrument. Installation and three-day training were included. Two faculty members in the Chemical and Materials Engineering Department purchased accessories to perform SAXS measurements from other funds (not related to this contract).

All funds awarded in this contract were expended for acquisition, installation, and indirect costs. One graduate student supported by the National Science Foundation and one undergraduate student

supported by the Louis Stokes Alliance for Minority participation at NMSU assisted with site preparation, installation, maintenance, and configuration of the instrument for users.

Table I: Configuration of the NMSU PANalytical Empyrean diffractometer.

System	Component	Purpose and characteristics
Incident beam optics	Divergence slits	Highest intensity; $K_{\alpha 1}$, $K_{\alpha 2}$, K_{β} radiation
	Bragg-BrentanoHD	Better resolution for powder measurements
	Ge (220) 2-bounce hybrid mono-chromator (mirror); 1.2 mm beam height	High-resolution measurements 26" FWHM for Si (111) Monochromatic beam (only $K_{\alpha 1}$)
Sample stages	Triple-axis stage ω, 2θ, χ, ϕ, z	Large samples, transmission measurements (SAXS)
	Five-axis stage ω, 2θ, χ, ϕ, z, x, y	Small samples, wafer mapping
Diffracted beam optics	Parallel plate collimator 0.27°	x-ray reflectance
	Three-bounce Ge (220) monochromator, 12" acceptance	Highest-resolution diffraction and reciprocal space maps
	Programmable anti-scatter slit	For linear detector
Detectors	Xe proportional detector; Programmable pneumatic beam attenuator (Ni 0.125 mm)	Single-channel (0D) detector for high-resolution triple-axis and reflectance measurements
	Pixcel 1D linear detector, 255 channels, 2.5° field of view (2θ)	Fast powder diffraction and reciprocal space maps
Software	Data Collector	Data acquisition
	Data Viewer	Display of data sets
	Highscore Plus	Search/Match with ICDD PDF database
	Epitaxy	Analysis and fitting of high-resolution diffraction data; display of reciprocal space maps
	Smoothfit	Plug-in for automated fitting
	Reflectivity	Analysis and fitting of reflectance data
	EasySAXS	Analysis of SAXS data
	Texture	Analysis of texture data

Table II: Level of NSMU expertise in various techniques on Empyrean instrument.

Technique	**NMSU experience level**
Powder diffraction	Mature
X-ray reflectance	Good (instrument issues)
High-resolution diffraction	Mature
Asymmetric reflections	Good
Reciprocal space maps	Mature
Triple-axis measurements	Good (instrument issues)
Small angle scattering	Not yet demonstrated
Texture, pole figures	Not yet demonstrated
Crystallography	Good
Non-cubic crystals	Basic

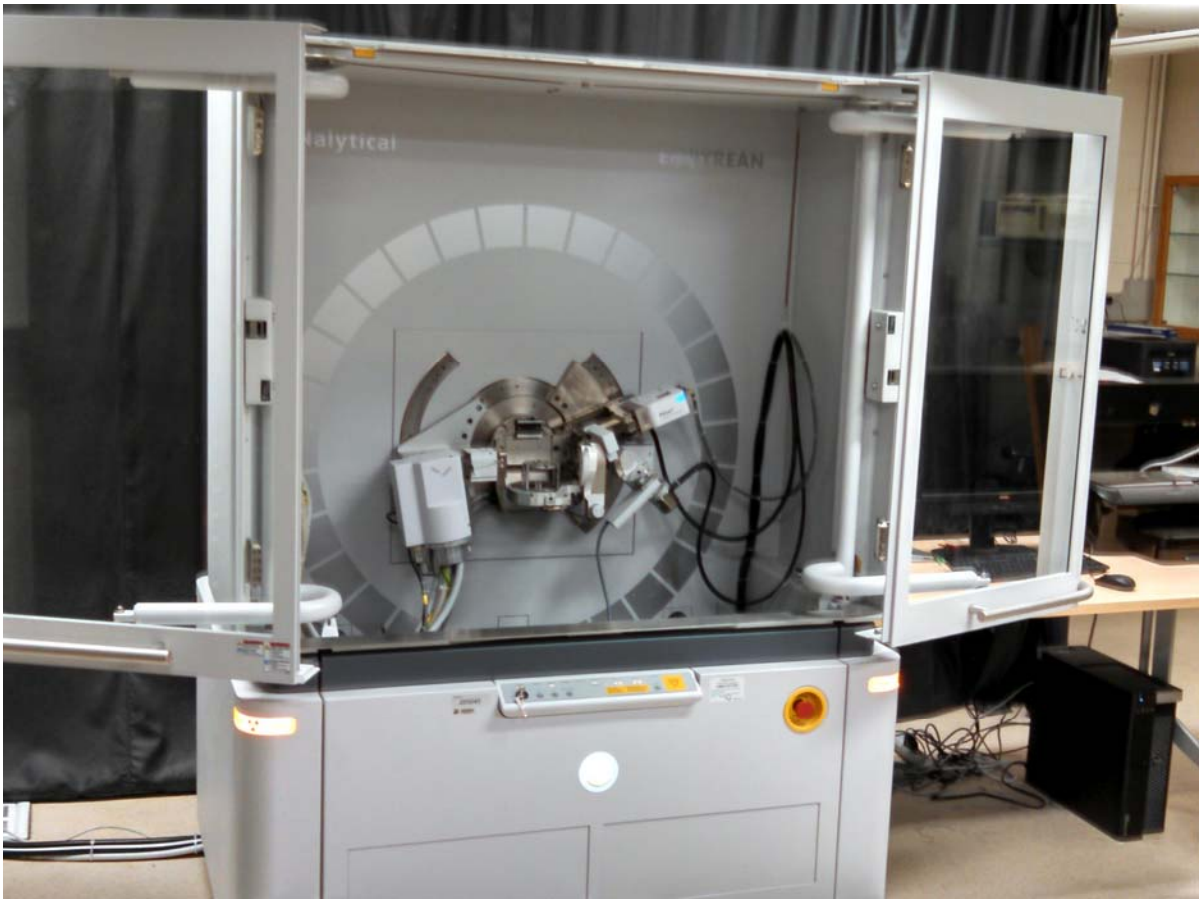

Figure 1: The NMSU Empyrean x-ray diffractometer in the PI's laboratory in Gardiner Hall.

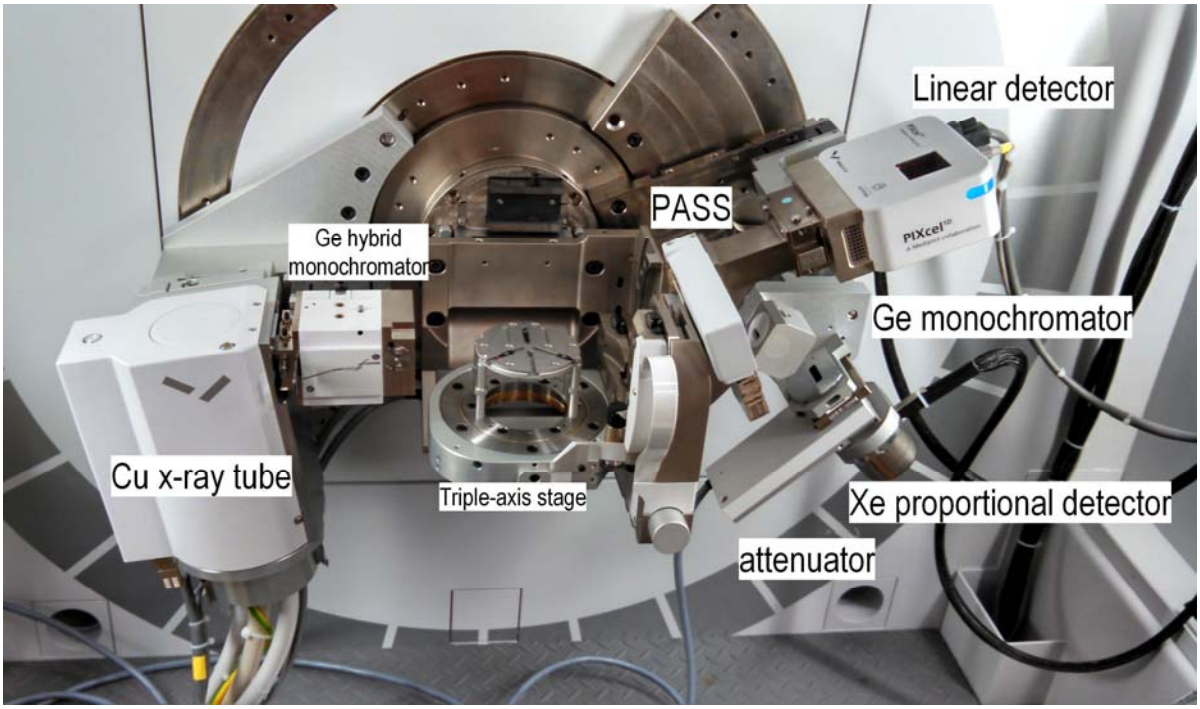

Figure 2: Close-up of the Empyrean diffractometer with x-ray optics configured for high-resolution powder diffraction and triple-axis reciprocal space maps.

Management

The instrument is owned and managed by the NMSU Office of the Vice President for Research, represented by Dr. Peter Cooke, Director of the Core University Research Resources Laboratory (CURRL), and a faculty advisory group, consisting of the PI (Stefan Zollner) and faculty from the Departments of Physics (Heinz Nakotte, Edwin Fohtung) and Chemical and Materials Engineering (Hongmei Luo, Reza Foudazi).

To use the instrument, users must submit a one-page user proposal, signed by a faculty sponsor, to the faculty advisory group describing the goals and outcomes of their experiment, the required instrumental configuration, and the materials to be measured. The advisory group will approve the proposal if the proposed experiment is feasible, a funding source can be identified to pay for the instrument, and after consideration of relevant safety issues. Users must also complete the x-ray radiation safety training course offered by the NMSU Department of Enviromental Health and Safety. After approval is completed, users are able to book the instrument through a web based system. The PI's research group will configure the instrument for the users' needs. Training on instrument use, experimental strategies, and data analysis must be provided by the users' faculty sponsor. Relevant training materials from the supplier have been posted on a Google Drive folder for authorized NMSU x-ray users. For data analysis, a computer has been set up for public use in the Physics computer lab in Gardiner Hall (GN 264). Users receive key card access to Gardiner Hall, the x-ray laboratory (GN 254), and the computer lab. External users from other universities, government labs, and private users are encouraged to submit user proposals.

Use of the instrument is currently charged at USD 20.00 per hour, with a maximum of USD 2000 (100 hours) per research group for each fiscal year (July through June). The fee will be adjusted annually as needed to raise funds for maintenance of the instrument and training of users. As of July 2015, 23 users have been authorized, including 5 faculty members, 15 graduate students, and 3 undergraduate students. Table III shows the use of the instrument during the 2014/15 fiscal year for various purposes, along with funding sources.

Table III: Overview of XRD instrument use during the 2014/15 fiscal year.

Type	Hours	Fees (USD)	Funding Source	Project
Instructional	26	510	Engineering student technology fee	PHYS 315L instructional laboratory (modern physics)
Undergraduate Research	48	960	Associate Dean for Research, College of Engineering	Crystal structure of complex metal oxides
Research	100+	2000	Federal grant	Ferroelectrics
Research	100+	2000	Federal grant	Germanium-tin alloys
Tech transfer	9	180	Startup company	Metallurgy
Research	5	100	Federal grant	SAXS
Total	300+	**5750**		

Instructional Use

In the spring semester of 2015, the x-ray diffractometer was used for a four-week long group project in the sophomore-more level instructional laboratory course PHYS 315L Experimental Modern Physics (taught by Dr. Stephen F. Pate, assisted by senior undergraduate Amber A. Medina). Excerpts from a report written by the students in this group are provided in Appendix A, with edits kept to a minimum to show the level of the students' learning. Appendix B shows sample spectra for poly- and single-crystalline Si to document the resolution of the instrument, especially with the Pixcel linear detector.

In the fall of 2015, the PI will teach a course PHYS 450/520 Special Topics: Elements of X-ray Diffraction. This course is offered for upper-division undergraduate students and beginning graduate students in physics and chemical and materials engineering. It is expected that this course will receive a regular course number for future offerings. The technical goals for this course are to develop an ability to acquire x-ray diffraction and reflectivity spectra and to understand the results for a materials system of interest to the student. Topics: (1) X-ray sources and detectors: Atomic spectra, characteristic x-rays, thermionic emission, synchrotron radiation. (2) Crystallography: Bravais lattice, basis, point and space group, Bragg planes, Miller indices, form and structure factor, reciprocal space, Bragg's Law. (3) Applications: Common lattice structures. (4) Epitaxial strained layers, Vegard's Law. (5) Instrument components: slits, mirrors, beam conditioners, detectors. (6) Experimental strategies: powder diffraction, $\omega/2\theta$, rocking curves, reciprocal space maps (symmetric and asymmetric), x-ray reflectance. Sample alignment. (7) Data analysis software. The text books will be selected by each student individually, based on interested, from the following: Powder XRD: Cullity&Stock, *Elements of X-Ray Diffraction*, 3rd edn, Pearson, ISBN 0201610914, USD 190; High-res XRD: Bowen&Tanner, *High Resolution X-Ray Diffractometry and Topography*, Taylor&Francis, ISBN 0850667585, USD 97; XRR&RSM: Holy, Pietsch&Baumbach, *High-Resolution X-Ray Scattering: From Thin Films to Lateral Nanostructures,* 2nd edn, Springer, ISBN 0387400923, USD 88; Elasticity&Crystallograpy: Irene, *Electronic Materials Science*, Wiley, ISBN 0471695971, USD 52; Rohrer, *Structure and Bonding in Crystalline Materials*, Cambridge University Press, ISBN 0521663792, USD 61. Crystal Structure: Kittel, *Introduction to Solid-State Physics*, Wiley, 8th edn, ISBN 047141526X USD 125. Students will also read selected journal articles or chapters, which will be posted on Canvas. Wikipedia and Google are also often excellent sources of information.

Students in PHYS 450/520 will be encouraged to gain practical experience on this instrument outside of class time with a project of their choice. This project will be the subject of a term paper (worth 40% of the course grade), which must be written in the format of a peer-reviewed journal manuscript.

Research Projects

The PI has a current research interest, supported by the National Science Foundation, related to the lattice dynamics and electronic band structure of complex metal oxides in bulk and thin-film form, including complex oxide heterostructures. Of special interest are the interactions between magnetic

ordering and phonon energies; and the band ordering of itinerant and localized electrons. (Compare Research Topic 6.1.1: Strong Correlations and Novel Phases of Matter of the Army Research Office BAA.) Since lattice dynamics and electronic band structure are intimately related to the crystal structure, the new x-ray diffractometer will see much use for this application to complex oxides.

As an example, Appendix C compares the crystal structure of LiF and NiO in powder and single-crystal form. Both LiF and NiO powders show the rocksalt structure and peaks in similar positions. The line widths of NiO $\omega/2\theta$ powder diffraction scans are larger than for LiF, because the NiO powder consists of smaller grains. The expected peak splitting due to the rhombohedral distortion of NiO (induced by antiferromagnetic ordering) is not visible in the NiO powder. This is consistent with the general statement that powders of nanoparticles prefer the high-symmetry phase over the distorted lower-symmetry phases. On the other hand, high-resolution $\omega/2\theta$ diffraction scans of single-crystalline LiF and NiO cut perpendicular to the (cubic) c(111) axis, obtained using the triple-axis diffracted beam optic, clearly show the splitting of the cubic (222) Bragg peak into hexagonal (202) and (006) peaks due to the rhombohedral distortion. Rocking curves of the LiF c(222) Bragg reflection show that the LiF single crystal shows multiple domains. The domain structure is even more complex for the NiO single crystal, as should be expected based on the four T-domains in antiferromagnetic NiO.

Appendix D summarizes x-ray diffraction results obtained from pseudomorphic $Ge_{1-x}Sn_x$ alloys grown on Ge using molecular beam epitaxy. This work was performed in collaboration with the group of Professor Kolodzey at the University of Delaware, Newark, and funded by the Air Force Office of Scientific Research under a grant with the title “(HBCU) Optical Spectroscopy of Materials for Group-IV Optoelectronics” and number FA9550-13-1-0022. Because of the high quality of these pseudomorphic epitaxial layers, we are able to demonstrate the highest-resolution measurements using the triple-axis Ge monochromator and the Xe proportional detector. Excellent results can also be obtained using the Pixcel linear detector, which reduces the data acquisition time by an order of magnitude with only slight reduction in data quality.

Appendix E shows the application of the instrument for x-ray reflectivity measurements of $SrTiO_3$ thin films on Si and Ge grown by molecular beam epitaxy.

Appendix A: Instrument use for instructional laboratory
PHYS 315L: Experimental Modern Physics

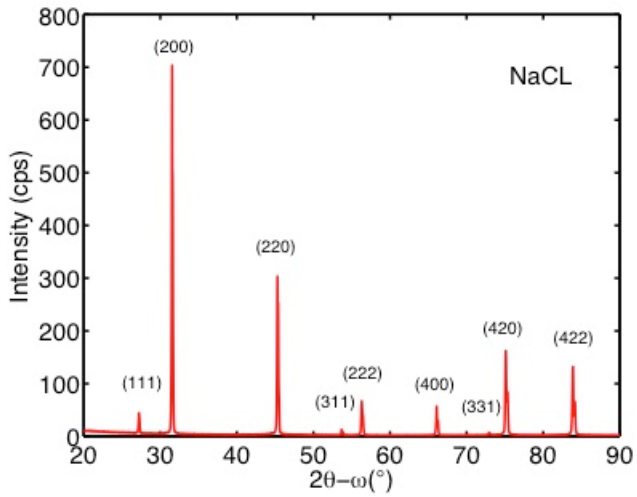

Figure A.1 is a 2θ-ω scan of NaCl powder. The incident optic used was the Bragg-Brentano HD optic with a 1/2° divergent slit and a 4 mm mask. The diffracted beam optic was the Pixcel1D detector with a 0.4 rad Soller slit, programmable anti-scatter slit, and a nickel filter.

Table A.I: Lattice constant measurements for NaCl (using powder).

NaCl Powder					
Peak	**FWHM**	**d (Å)**	**Δd (Å)**	**a_o (Å)**	**Δa_o (Å)**
(111)	0.17	3.271	0.015	5.67	0.03
(200)	0.15	2.833	0.011	5.67	0.02
(220)	0.20	2.000	0.010	5.66	0.03
(311)	0.24	1.706	0.009	5.66	0.03
(222)	0.26	1.632	0.010	5.65	0.04
(400)	0.12	1.412	0.004	5.65	0.02
(331)	0.17	1.296	0.005	5.65	0.02
(420)	0.17	1.263	0.005	5.65	0.02
(422)	0.16	1.152	0.004	5.65	0.02

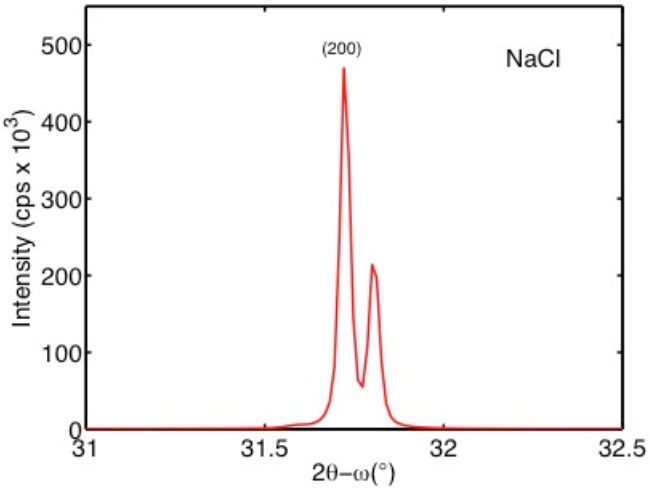

Figure A.2 is a 2θ-ω scan of a <100> NaCl single crystal. The incident optic used was the Bragg-Brentano HD optic with a 1/2° divergent slit and a 4 mm mask. The diffracted beam optic was the Pixcel1D detector with a 0.4 rad Soller slit, programmable anti-scatter slit, and a nickel filter. The (200) peak can be seen splitting from the two different wavelengths of x-rays, $K_{\alpha 1}$ and $K_{\alpha 2}$, generated by the x-ray tube.

Table A.II: Lattice constant measurements for NaCl using a single crystal.

NaCl 100 Single Crystal					
Peak	**FWHM**	**d (Å)**	**Δd (Å)**	**a_o (Å)**	**Δa_o (Å)**
(200)	0.038	2.818	0.003	5.637	0.006

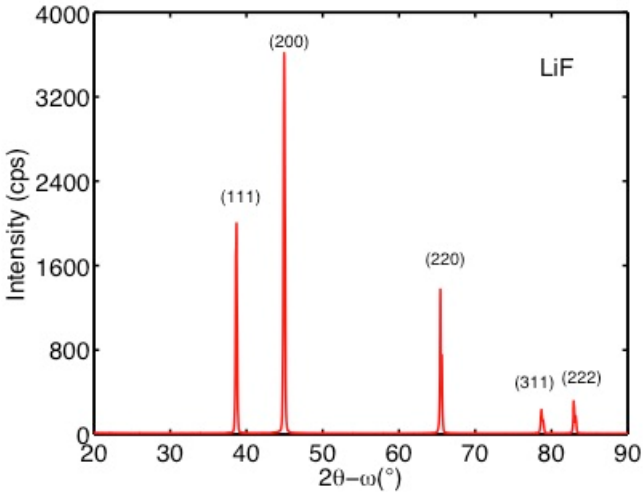

Figure A.3 is a 2θ-ω scan of LiF powder. The incident optic used was the Bragg-Brentano HD optic with a 1/2° divergent slit and a 4 mm mask. The diffracted beam optic was the Pixcel1D detector with a 0.4 rad Soller slit, programmable anti-scatter slit, and a nickel filter.

Table A.III: Lattice constant measurements for LiF (using powder).

LiF Powder					
Peak	**FWHM**	**d (Å)**	**Δd (Å)**	**a_o (Å)**	**Δa_o (Å)**
(111)	0.19	2.327	0.010	4.03	0.02
(200)	0.22	2.015	0.008	4.03	0.02
(220)	0.32	1.425	0.003	4.03	0.01
(311)	0.22	1.215	0.007	4.03	0.02
(222)	0.23	1.163	0.003	4.03	0.01

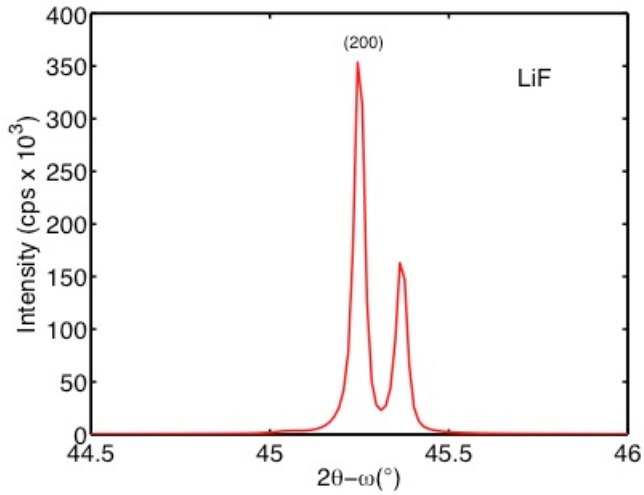

Figure A.4 is a 2θ-ω scan of a <100> LiF crystal. The incident optic used was the Bragg-Brentano HD optic with a 1/2° divergent slit and a 4 mm mask. The diffracted beam optic was the Pixcel1D detector with a 0.4 rad Soller slit, programmable anti-scatter slit, and a nickel filter. The (200) peak can be seen splitting from the two different wavelengths of x-rays, $K_{\alpha 1}$ and $K_{\alpha 2}$, generated by the x-ray tube.

Table A.IV: Lattice constant measurements for LiF using a single crystal.

LiF 100 Single Crystal					
Peak	**FWHM**	**d (Å)**	**Δd (Å)**	**a_o (Å)**	**Δa_o (Å)**
(200)	0.035	2.002	0.001	4.005	0.003

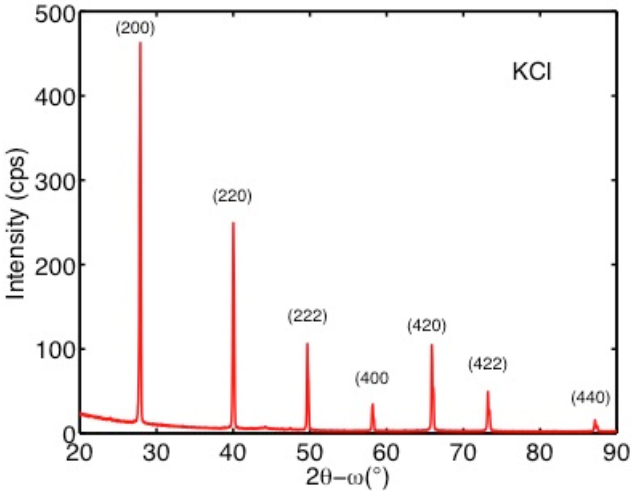

Figure A.5 is a 2θ-ω scan of KCl powder. The incident optic used was the Bragg-Brentano HD optic with a 1/2° divergent slit and a 4 mm mask. The diffracted beam optic was the Pixcel1D detector with a 0.4 rad Soller slit, programmable anti-scatter slit, and a nickel filter.

Table A.V: Lattice constant measurements for KCl (using powder).

KCl Powder					
Peak	**FWHM**	**d (Å)**	**Δd (Å)**	**a_o (Å)**	**Δa_o (Å)**
(200)	0.13	3.196	0.020	6.39	0.04
(220)	0.18	2.251	0.013	6.37	0.04
(222)	0.28	1.834	0.011	6.35	0.04
(400)	0.13	1.585	0.013	6.34	0.05
(420)	0.16	1.416	0.006	6.33	0.03
(422)	0.32	1.292	0.006	6.33	0.03
(440)	0.20	1.117	0.005	6.32	0.03

Appendix B: Resolution of linear (Pixcel) detector and application to poly-crystalline and single-crystalline Si

Authors: Jaime Moya and Nuwanjula Samarasingha

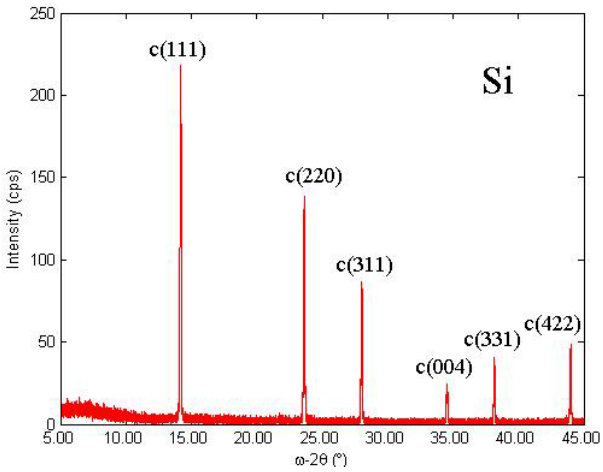

Figure B.1 is an ω-2θ scan of a silicon calibration powder disk. The incident beam configuration is the Ge hybrid monochromator with a 1/2° divergence slit and a 4 mm mask. The diffracted beam configuration is a Pixcel1D detector with a 0.4 rad Soller slit.

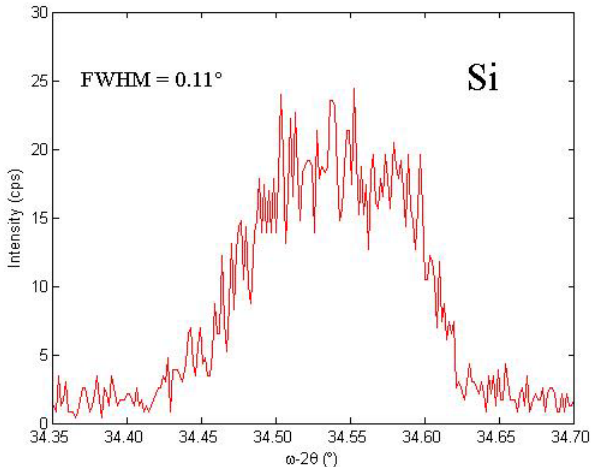

Figure B.2 is an ω-2θ scan zoomed in on the c(004) peak of a silicon calibration powder disk. The incident beam configuration is the Ge hybrid monochromator with a 1/2° divergence slit and a 4 mm mask. The diffracted beam configuration is a Pixcel1D detector with a 0.4 rad soller slit. The full width half maximum is 0.11°.

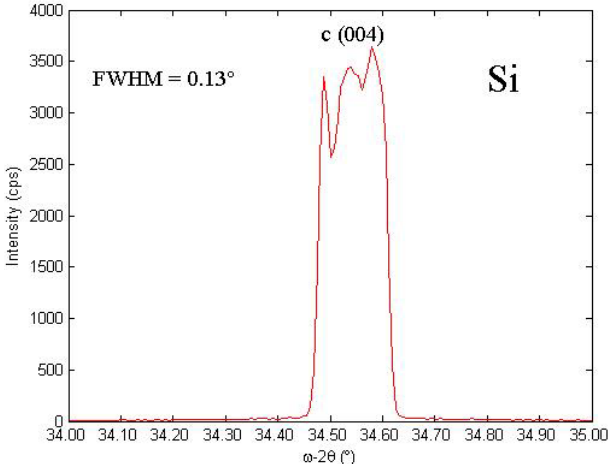

Figure B.3 is an ω-2θ scan of a c(004) silicon single crystal. The incident beam configuration is the Ge hybrid monochromator with a 1/2° divergence slit and a 4 mm mask. The diffracted beam configuration is a Pixcel1D detector with a 0.4 rad soller slit. The full width half maximum is 0.13°.

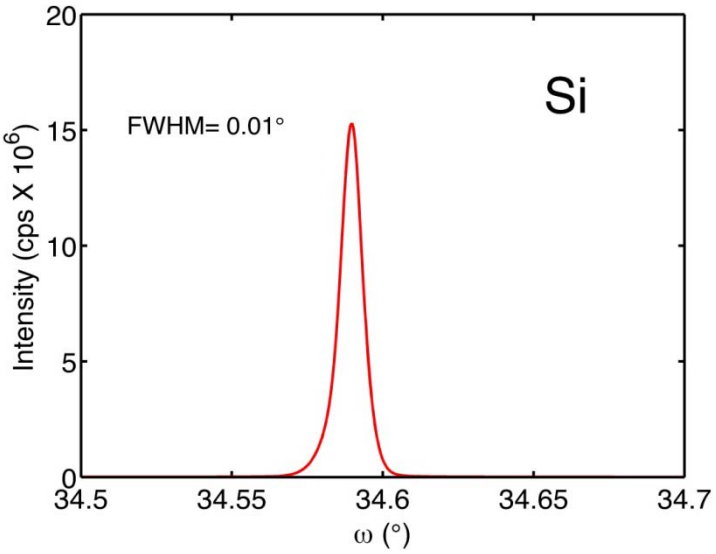

Figure B.4 is rocking curve (ω-scan) of the (004) peak in the silicon crystal. The incident beam configuration is the Ge hybrid monochromator with a 1/2° divergence slit and a 4 mm mask. The diffracted beam configuration is a Pixcel1D detector with a 0.4 rad soller slit. The full width half maximum is 0.01°. This is in reasonable agreement with the rocking curve FWHM of 0.007° specified for the Si (111) Bragg reflection.

Appendix C: Crystal structure difference between cubic rocksalt LiF and rhombohedrally distorted NiO

Authors: Jaime Moya and Nuwanjula Samarasingha

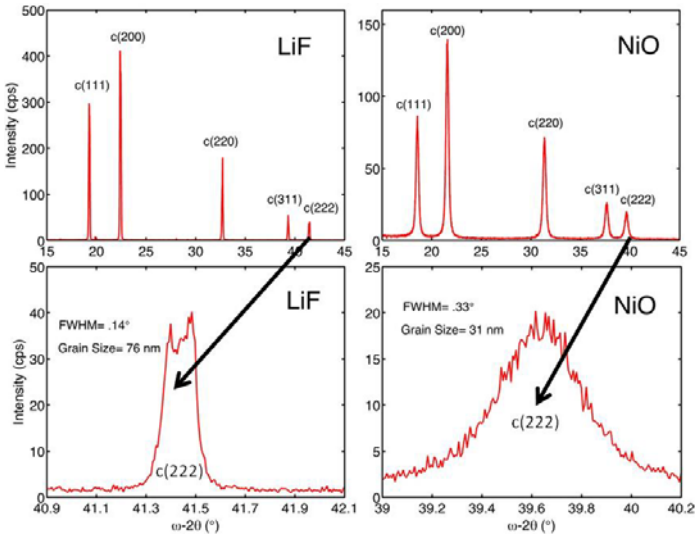

Figure C.1: Comparison of XRD spectra for LiF and NiO powders, showing the similarity of the two rocksalt crystal types. Data were taken using the Ge hybrid monochromator, programmable anti-scatter slit, and the Pixcel linear detector. The bottom panels zoom in on the (222) peaks of the rocksalt structure. No splitting of this peak is seen for NiO. The peak width is larger for NiO, because the grain size is smaller.

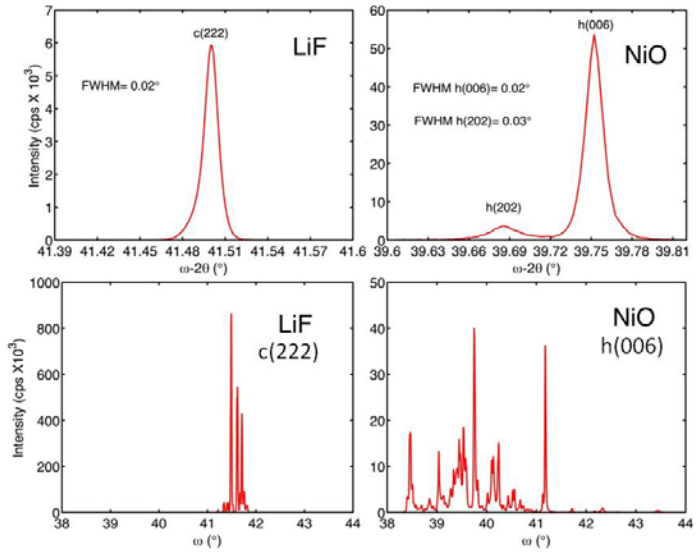

Figure C.2: Top: Comparison of $\omega/2\theta$ spectra for c(111)-oriented single-crystalline LiF and NiO, taken with the Ge hybrid monochromator, triple-axis diffracted beam optic, and the proportional detector. The prefixes c and h denote the cubic and hexagonal Miller indices, respectively. The rhombohedral splitting between h(006) and h(202) for NiO is clearly visible. Bottom: Rocking curves for the LiF c(222) and NiO h(006) Bragg reflections show that both single crystals have multiple domains. Because of twinning, the domain structure is more complicated for NiO.

Appendix D: High-resolution diffraction of $Ge_{1-x}Sn_x$ alloys grown pseuomorphically on Ge by molecular beam epitaxy

Author: Nalin Fernando and Stefan Zollner

To demonstrate the ability of the instrument to acquire high-resolution symmetric and asymmetric diffraction data, including reciprocal space maps (RSMs) in grazing exit geometry, we investigated several $Ge_{1-x}Sn_x$ alloys grown pseudomorphically on Ge (001) substrates using molecular beam epitaxy at University of Delaware. See pages 15 through 21.

The top left of each slide shows a symmetric (004) ω-2θ scan. Experimental data are shown in blue and the results of simulations (using the thickness and Sn content as parameters) in red. At ω=33°, we find the Ge (004) Bragg reflection. The $Ge_{1-x}Sn_x$ layer peak is shifted towards lower Bragg angles. From the separation of the two peaks, we calculate the out-of-plane lattice constant of the alloy c. For high-quality layers, the alloy peak width is transform-limited and a periodic set of thickness fringes appear on both sides of the alloy peak. For lower-quality samples, the alloy peak is broader and the thickness fringes are missing (SGC 581) or not as regular and periodic as they should be (SGC 684). Once the out-of-plane lattice constant c is known, we can calculate the Sn content if we make certain assumptions about the Poisson ratio of the alloy and the lattice constant bowing parameter b. Unfortunately, there is no agreement in the literature about the value of b and therefore we show two values for the Sn content in each table.

On the top right of each slide, we show symmetric (004) RSMs in reciprocal space coordinates, taken with the Pixcel line detector (fast acquisition, a few hours) or with the Xe proportional detector (slow acquisition, 10 hours or more). The vertical axis q_y is related to the out-of-plane lattice constant c, again showing an increasing separation of substrate peak (top) and alloy peak (bottom) with clear thickness fringes. The horizontal axis q_x is related to a potential tilt between the epilayer and the Ge substrate. This tilt is very large for SGC 581 and also visible for SGC 687. It is likely that this tilt is influenced by the growth temperature and the substrate miscut.

In the bottom left, we show (224) RSMs taken under grazing exit (g.e.) condition in reciprocal space coordinates. For all samples, the alloy epilayer peak is located directly below the substrate peak, indicating pseudomorphic strain. For most samples, thickness fringes are also visible. From these (224) g.e. RSMs, we determined both the in-plane (a) and out-of-plane lattice constants for the substrate and epilayer, shown in the tables on the bottom right. Probable errors in the reciprocal space coordinates and lattice constants are shown in parentheses. In the right column of the table, we show the relaxed lattice constant of the alloy, which may show slight variations because of different assumptions of the compositional dependence of the Poisson ratio.

Slide 22 shows on the vertical axis the out-of-plane strained (red) and resulting relaxed (black) lattice constants of the alloys determined from the (224) grazing exit reciprocal space maps. On the horizontal axis, we show the Sn concentration determined from the (004) ω–2θ scans for each sample. There are

two different tin constants given for each sample. The solid lines assume a bowing parameter b=0.166, while the dashed lines assume that Vegard's Law is valid (b=0). The ovals enclose the data points calculated using Vegard's Law.

On page 23, we show the in-plane (black) and out-of-plane (red) strains calculated for each sample. The hydrostatic and shear strains are shown in blue and green, respectively. Again, there are two sets of data. The solid lines assume a bowing parameter of 0.166, while the dashed lines assume that Vegard's Law is valid. These strain parameters are important, because they are used as input to calculate band gaps in $Sn_{1-x}Ge_x$ alloys. This will be the topic of a forthcoming journal article.

SGC581: $Ge_{98}Sn_2$ on Ge

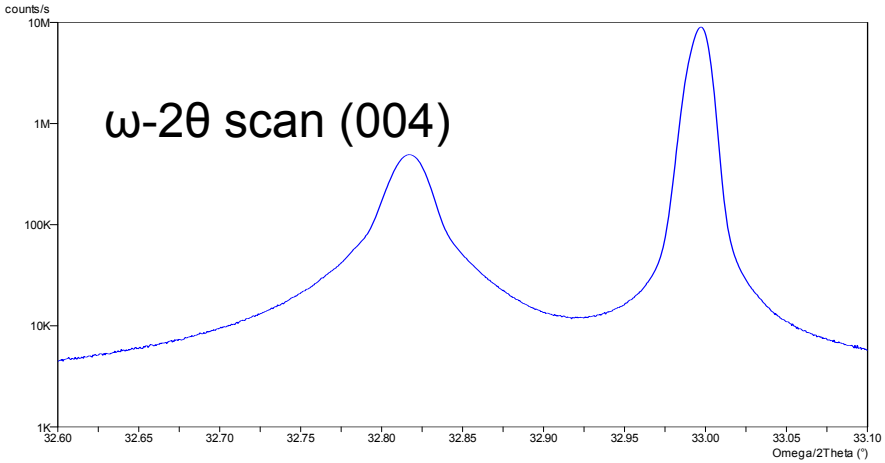

RSM(004)

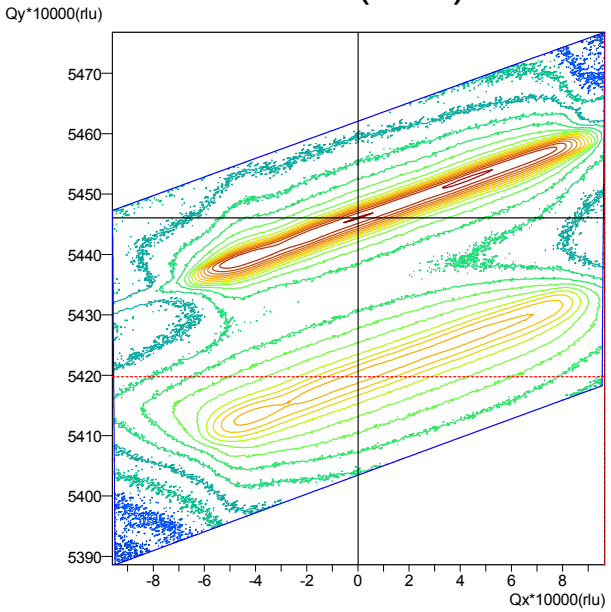

	UDEL	b=0	b=0.166
Sn content	0.02	0.019	0.016
	UDEL	**XRD**	**Ellipsometry**
Thickness (nm)	324		344

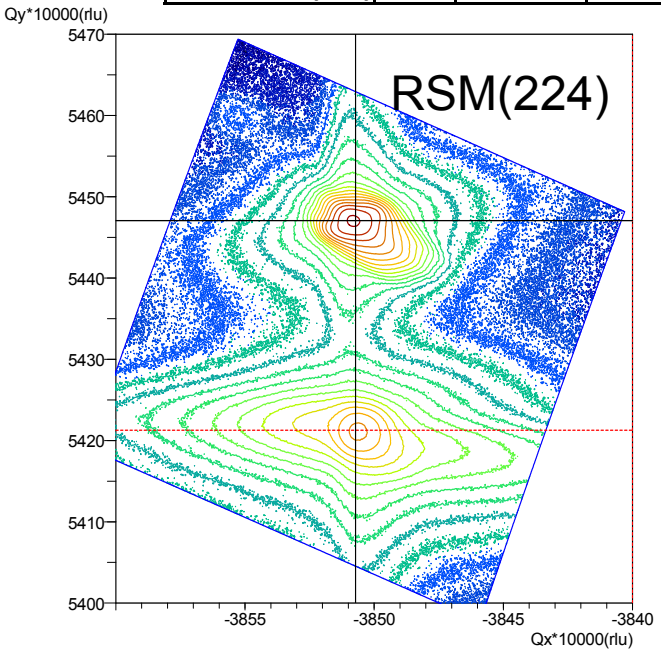

(224)	Ge	$Ge_{98}Sn_2$	relaxed $Ge_{98}Sn_2$
q_y (rlu)	0.5447(1)	0.5421(2)	b=0.166; 5.670(2)
c(Å)	5.657(1)	5.684(2)	
q_x (rlu)	-0.38508(5)	-0.38506(6)	b=0; 5.673(2)
a(Å)	5.6579(8)	5.6582(9)	

With PIXcel detector

rlu=2/λ=2/1.5406 $Å^{-1}$

SGC686: $Ge_{93.2}Sn_{6.8}$ on Ge

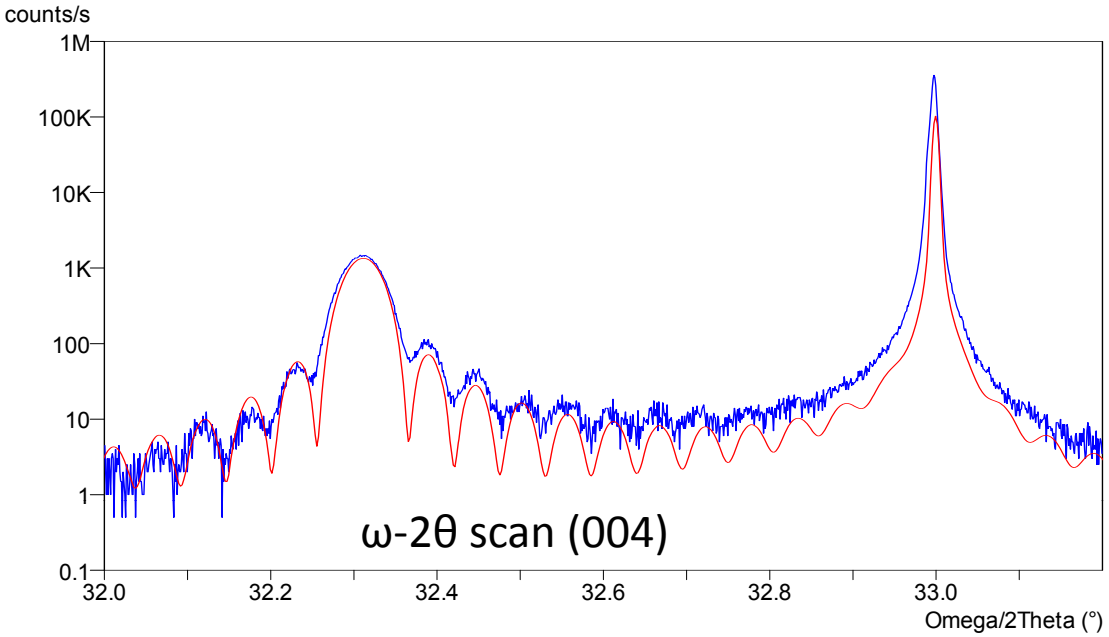

RSM(004)

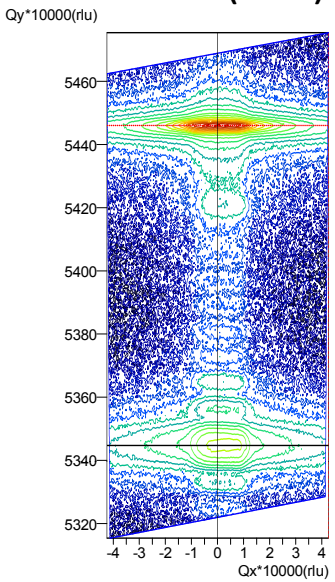

	UDEL	b=0	b=0.166
Sn content	0.068	0.074	0.062
	UDEL	**XRD**	**Ellipsometry**
Thickness (nm)	~93	98	

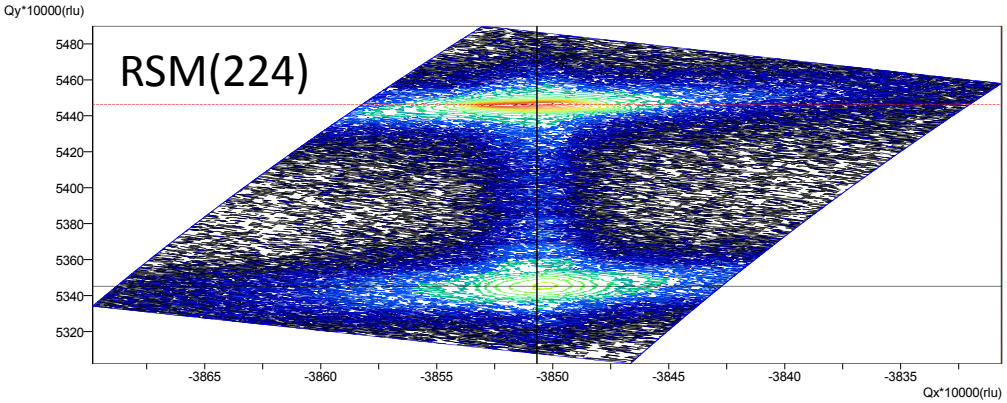

With Proportional detector

(224)	Ge	$Ge_{93.2}Sn_{6.8}$	relaxed $Ge_{93.2}Sn_{6.8}$
q_y (rlu)	0.54460(8)	0.5346(3)	b=0.166; 5.719(3)
c(Å)	5.6577(8)	5.76378(8)	
q_x (rlu)	-0.3851(1)	-0.3850(1)	b=0; 5.719(3)
a(Å)	5.657(1)	5.659(2)	

rlu=2/λ=2/1.5406 $Å^{-1}$

SGC689: $Ge_{92.8}Sn_{7.2}$ on Ge

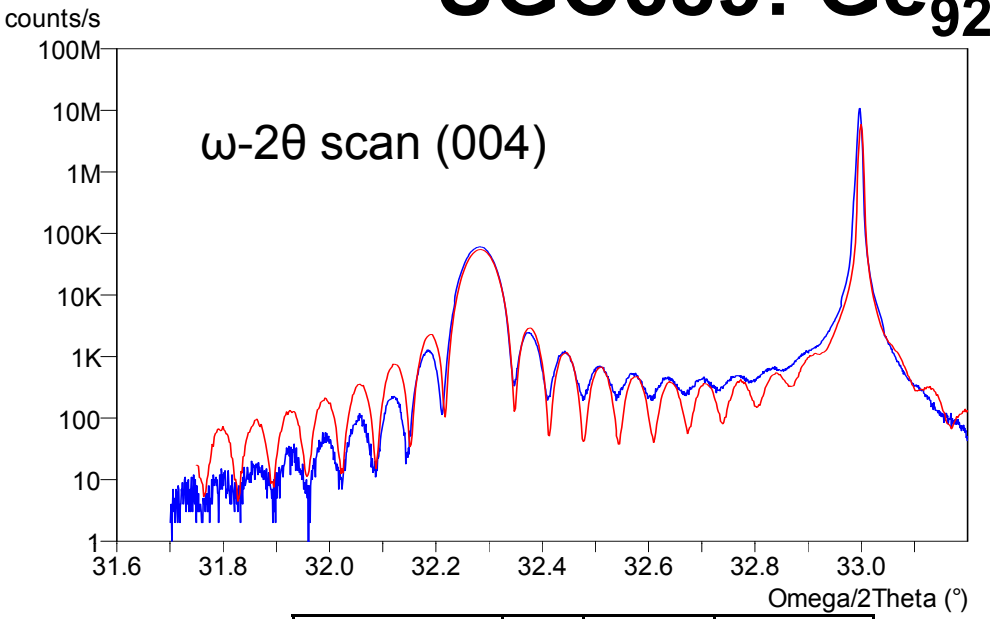

RSM(004)

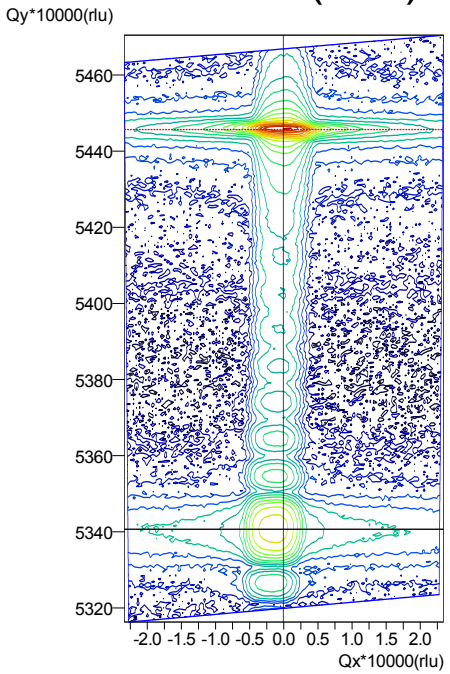

	UDEL	b=0	b=0.166
Sn content	0.072	0.076	0.064
	UDEL	**XRD**	**Ellipsometry**
Thickness (nm)	81	81	89.6

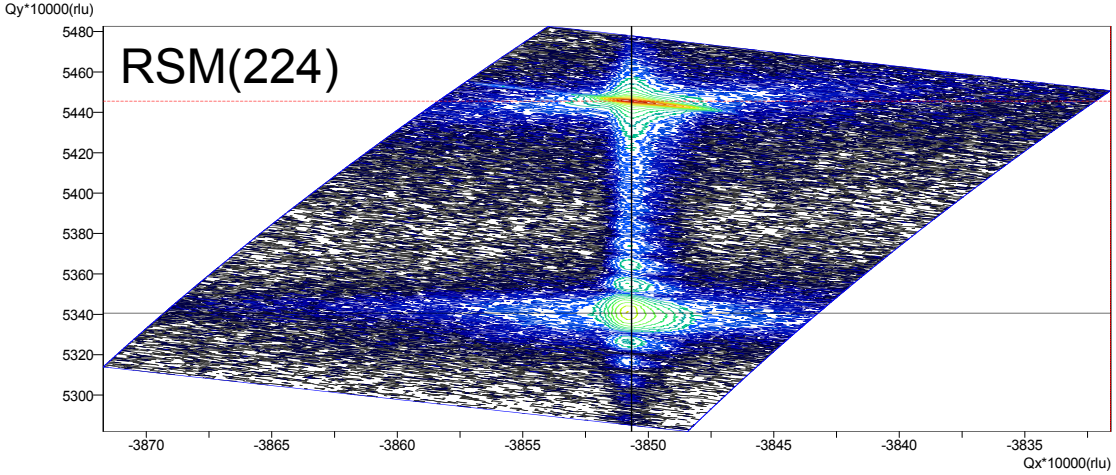

(224)	Ge	$Ge_{92.8}Sn_{7.2}$	relaxed $Ge_{92.8}Sn_{7.2}$
q_y (rlu)	0.54458(4)	0.5341(3)	b=0.166; 5.721(2)
c(Å)	5.6580(4)	5.768(3)	
q_x (rlu)	-0.38508(2)	-0.38510(3)	b=0; 5.721(2)
a(Å)	5.6578(3)	5.6576(4)	

rlu=2/λ=2/1.5406 $Å^{-1}$

With Proportional detector

SGC687: $Ge_{92.7}Sn_{7.3}$ on Ge

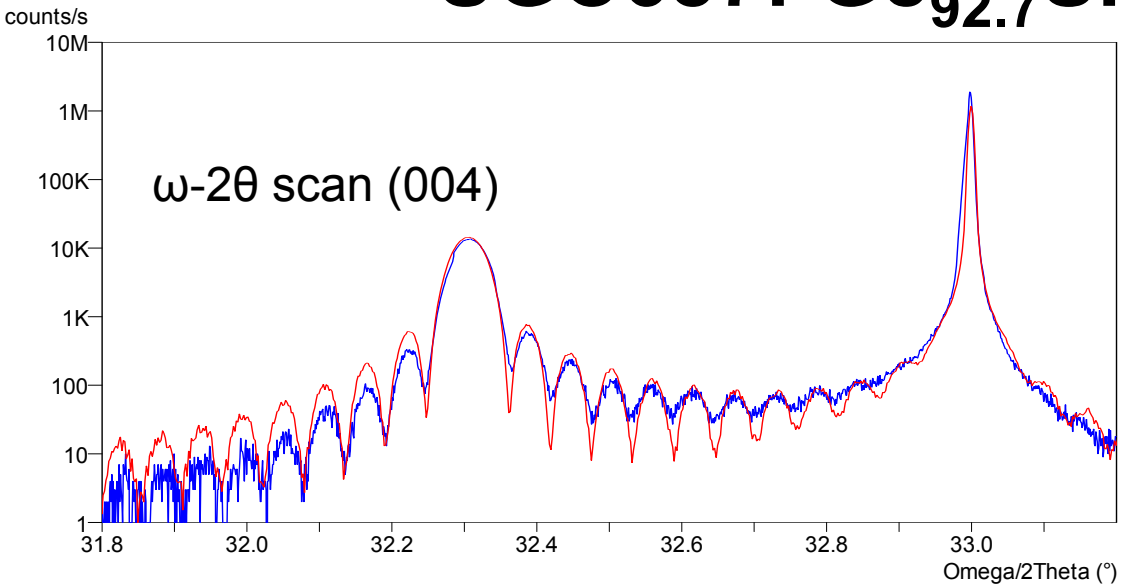

	UDEL	b=0	b=0.166
Sn content	0.073	0.073	0.061
	UDEL	**XRD**	**Ellipsometry**
Thickness (nm)	~94	92	92.3

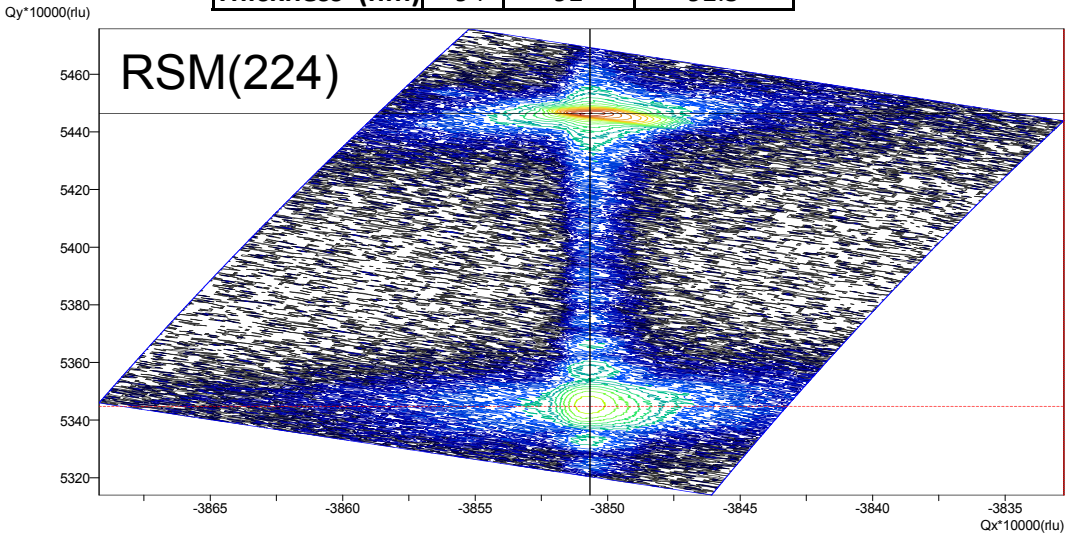

With Proportional detector

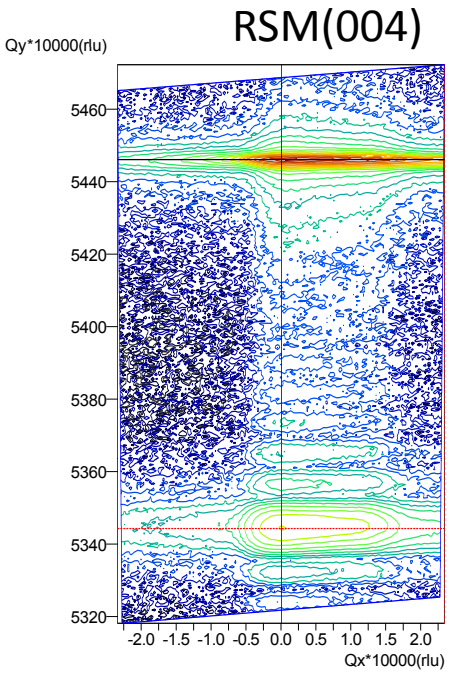

(224)	Ge	$Ge_{92.7}Sn_{7.3}$	relaxed $Ge_{92.7}Sn_{7.3}$
q_y (rlu)	0.54461(7)	0.5346(3)	b=0.166; 5.718(2)
c(Å)	5.6584(7)	5.765(4)	
q_x (rlu)	-0.38509(5)	-0.38506(6)	b=0; 5.718(2)
a(Å)	5.6578(8)	5.6582(9)	

rlu=2/λ=2/1.5406 $Å^{-1}$

SGC685: $Ge_{92.5}Sn_{7.5}$ on Ge

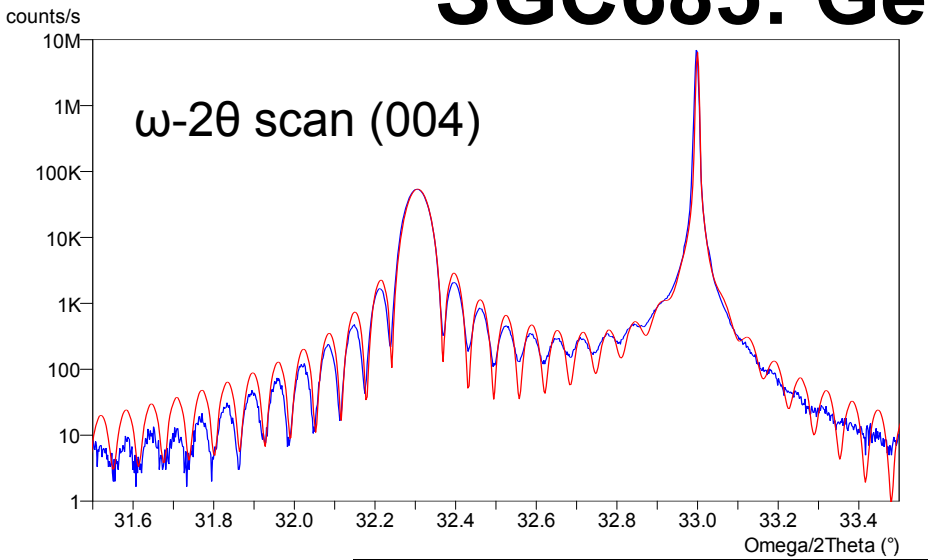

	UDEL	b=0	b=0.166
Sn content	0.075	0.075	0.063
	UDEL	**XRD**	**Ellipsometry**
Thickness (nm)	~90	83	83.5

RSM(004)

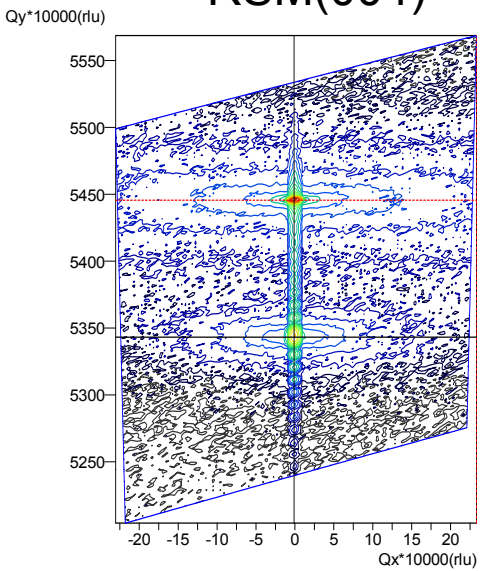

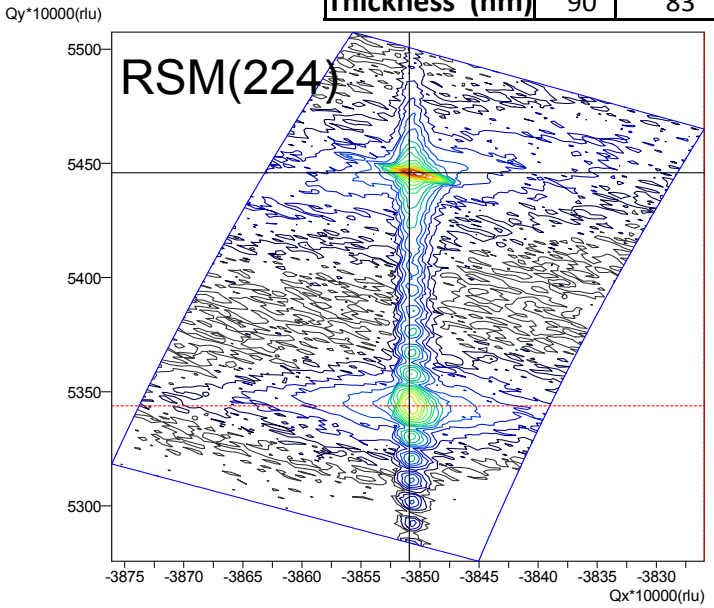

(224)	Ge	$Ge_{92.5}Sn_{7.5}$	relaxed $Ge_{92.5}Sn_{7.5}$
q_y (rlu)	0.54459(7)	0.5346(4)	b=0.166; 5.718(3)
c(Å)	5.6578(7)	5.763(5)	
q_x (rlu)	-0.38509(3)	-0.38509(7)	b=0; 5.718(3)
a(Å)	5.6577(5)	5.658(1)	

rlu=2/λ=2/1.5406 $Å^{-1}$

With Proportional detector

SGC693: $Ge_{90.3}Sn_{9.7}$ on Ge

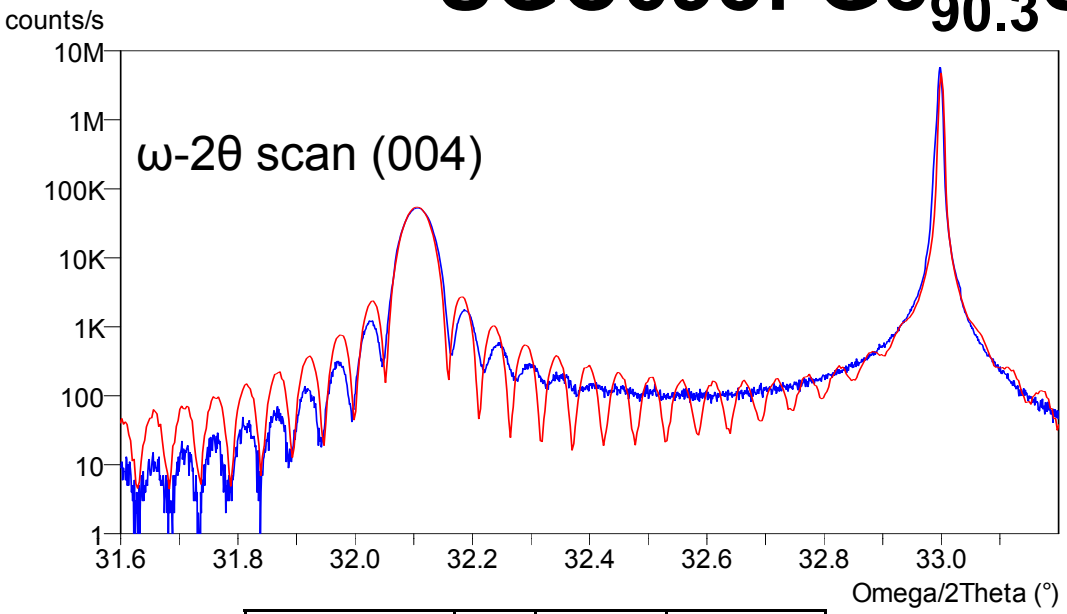

	UDEL	b=0	b=0.166
Sn content	0.097	0.096	0.0811
	UDEL	XRD	Ellipsometry
Thickness (nm)	104	93	104

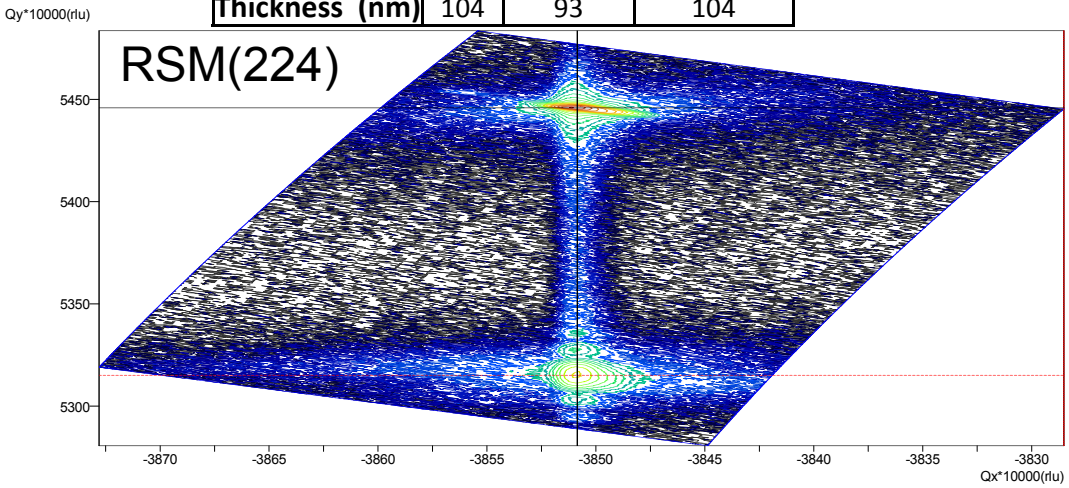

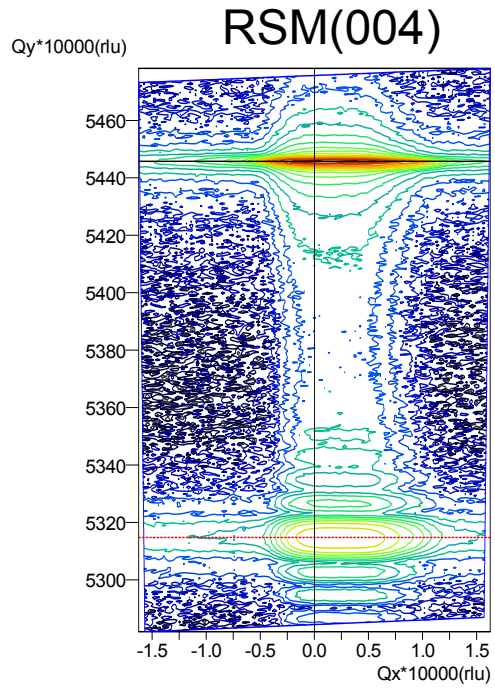

(224)	Ge	$Ge_{90.3}Sn_{9.7}$	relaxed $Ge_{90.3}Sn_{9.7}$
q_y (rlu)	0.54461(6)	0.5315(3)	
c(Å)	5.6577(7)	5.797(3)	b=0.166; 5.737(2)
q_x (rlu)	-0.38511(5)	-0.38509(5)	
a(Å)	5.6574(7)	5.6577(7)	b=0; 5.738(2)

rlu=2/λ=2/1.5406 $Å^{-1}$

With Proportional detector

SGC684: $Ge_{89}Sn_{11}$ on Ge

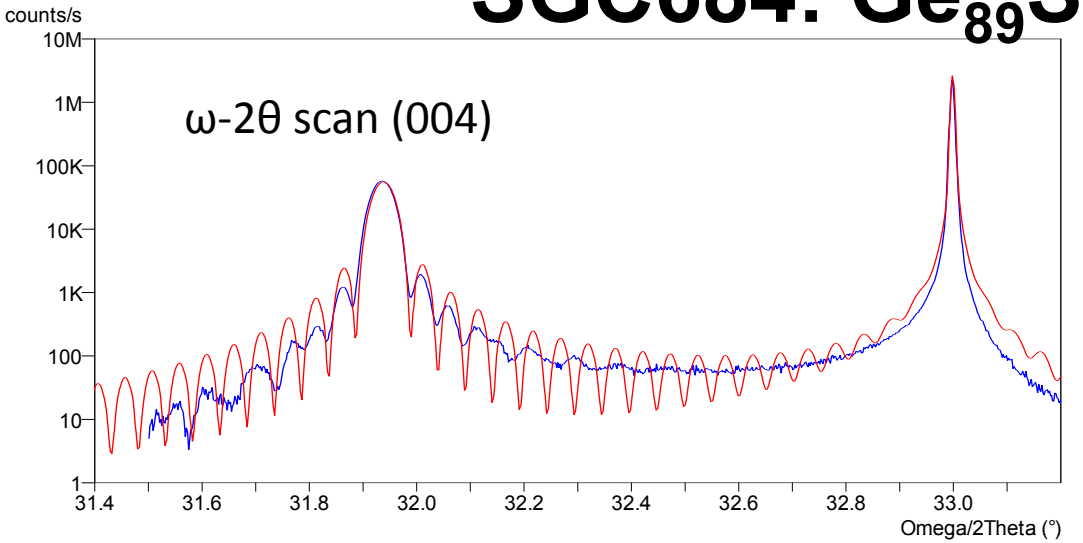

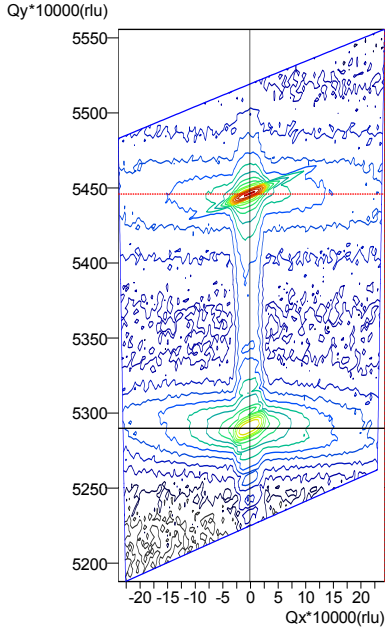

	UDEL	b=0	b=0.166
Sn content	0.11	0.11	0.097
	UDEL	**XRD**	**Ellipsometry**
Thickness (nm)	~109	101	115

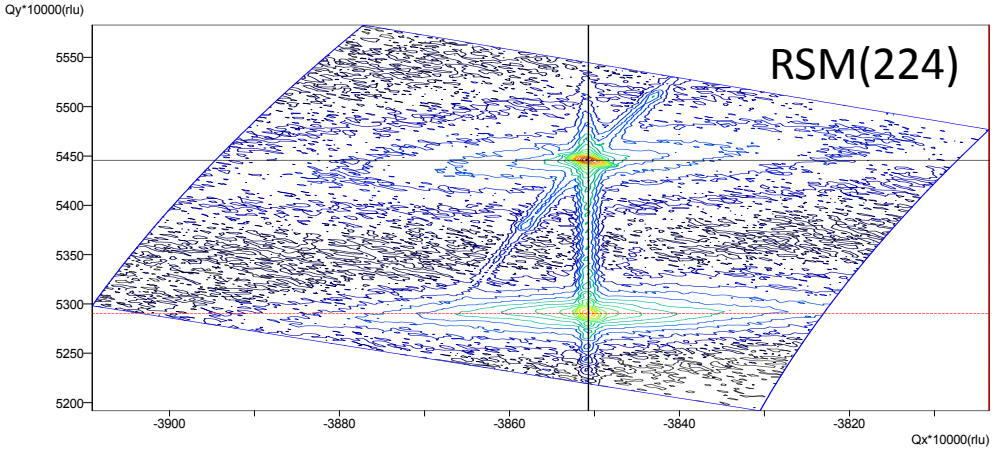

(224)	Ge	$Ge_{89}Sn_{11}$	relaxed $Ge_{89}Sn_{11}$
q_y (rlu)	0.5447(2)	0.5291(2)	b=0.166; 5.752(2)
c(Å)	5.657(2)	5.823(3)	
q_x (rlu)	-0.38508(5)	-0.38507(5)	b=0; 5.752(2)
a(Å)	5.6579(7)	5.6580(7)	

rlu=2/λ=2/1.5406 $Å^{-1}$

With PIXcel detector

Lattice parameters of $Ge_{1-y}Sn_y$ on Ge

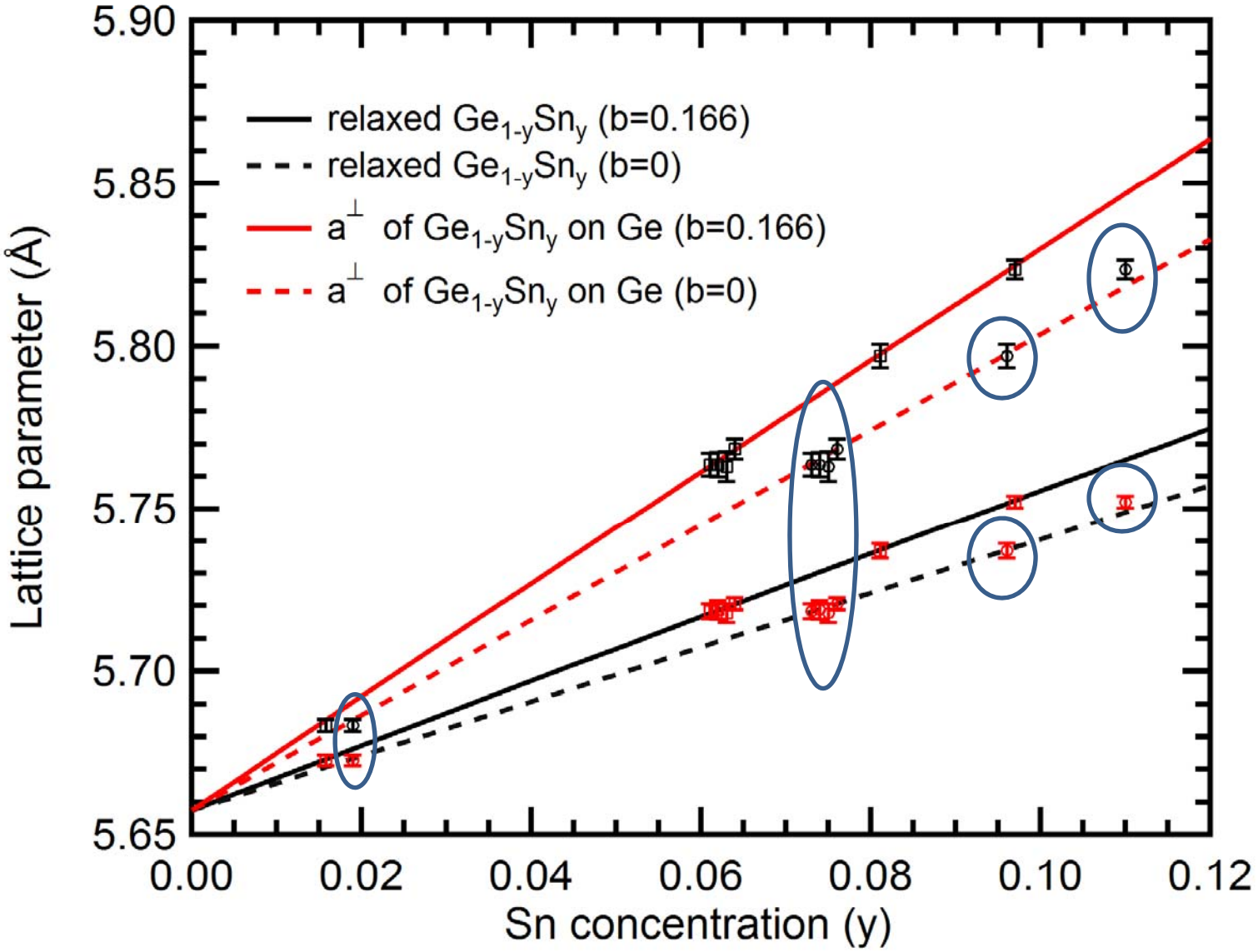

Strain of Pseudomorphic $Ge_{1-y}Sn_y$ on Ge

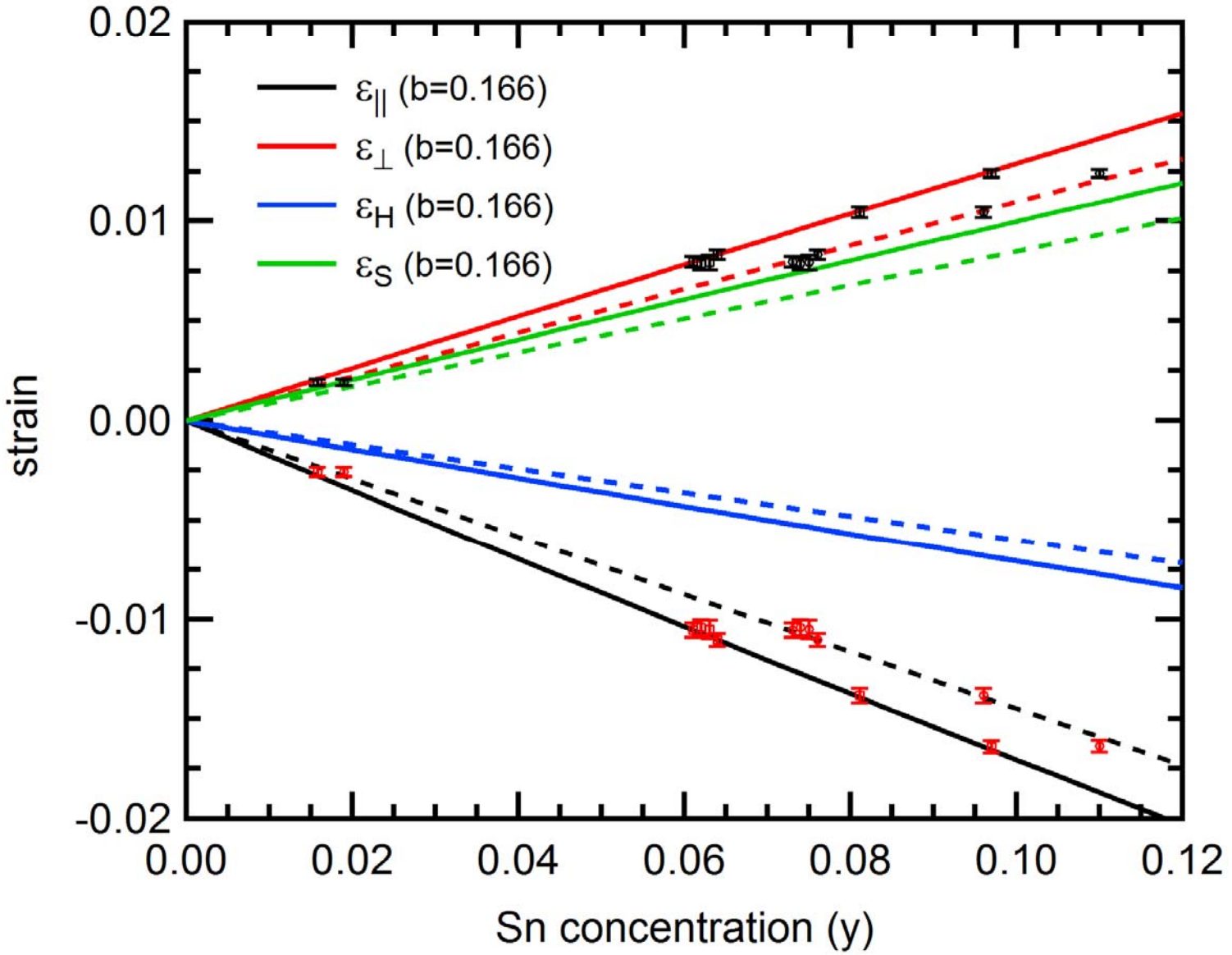

Appendix E: X-ray Reflectivity of MBE deposited Strontium Titanate (STO) thin films on two different substrates

Authors: Sudeshna Chattopadhyay, Nuwanjula S. Samarasingha Arachchige, and Jaime Moya

X-ray reflectivity (XRR) is a nondestructive technique to extract the electron density profile, surface-interface roughness, and film thickness (<100 nm) with high resolution. XRR data of $SrTiO_3$ films on different substrates (Si and Ge) are shown in Fig. E.1. These XRR data were taken using the Ge (220) 2-bounce hybrid monochromator with 1/32° divergence slit, 0.27° parallel-plate collimator with a 0.1 mm XRR slit, and the Xe proportional detector. The samples were grown using molecular beam epitaxy (MBE) by Professor Demkov's group, University of Texas at Austin.

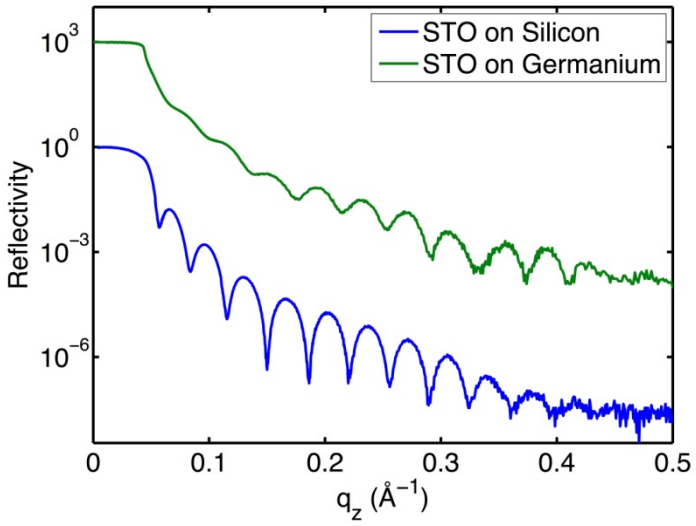

Figure E.1: Specular x-ray reflectivity data for strontium titanate, $SrTiO_3$ (STO), on different substrates (Si and Ge). Reflectivity data for STO on Si has been shifted up for clarity. A footprint correction was performed to avoid artifacts in the data at shallow angles due to the finite sample size. The horizontal axis is given in reciprocal space units $q_z=(4\pi\sin\theta)/\lambda$.

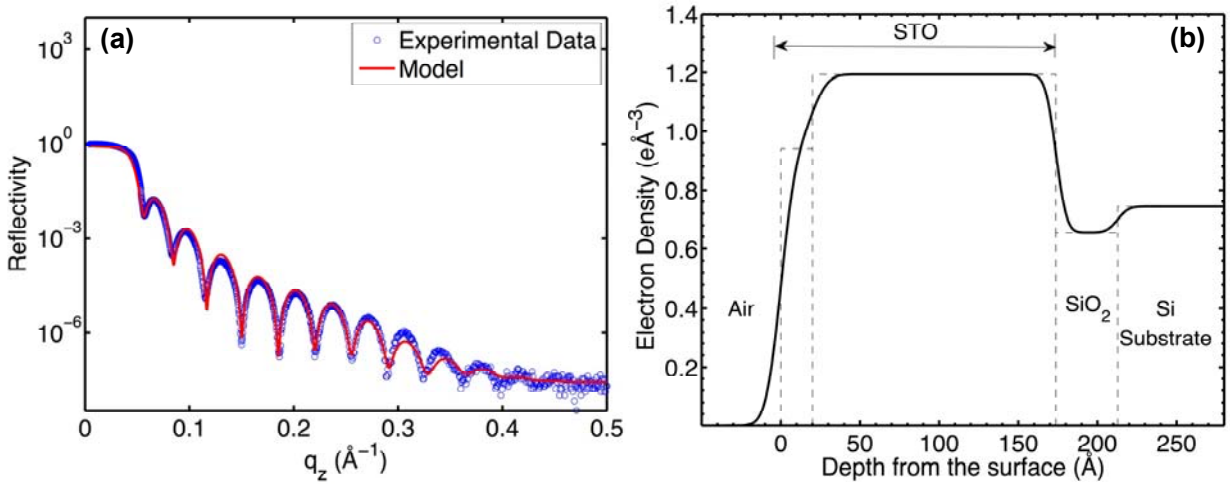

Figure E.2: (a) Specular reflectivity data for a STO film on silicon (blue symbols). The red line shows the best fit to the data using the electron-density profile shown in (b).

The XRR data were fitted using the Parratt formalism [1] to extract the electron density profile (EDP) of the system, i.e., the electron density as a function of film depth from the top surface, where the electron

density profile (EDP) is modeled as a series of uniform-density slabs connected by error-function interfaces to account for surface and interface roughness (see Fig. E.2).

Ref. 1: L.G. Parratt, Phys. Rev. **95**, 359 (1954).